

基于多层抗蚀剂的 GaAs 基微纳光栅深刻蚀工艺

杨晶晶^{*}, 范杰^{**}, 马晓辉^{**}, 邹永刚, 王琦琦

长春理工大学高功率半导体激光国家重点实验室, 吉林 长春 130022

摘要 采用电子束光刻技术制备出了深刻蚀的 GaAs 基微纳光栅。针对电子束曝光过程中存在的由邻近效应引起的光栅结构图形失真和变形的问题, 本课题组采用厚度较薄的 PMMA A4 抗蚀剂和 SiO₂ 薄膜形成多层抗蚀剂来减小邻近效应, 同时将 SiO₂ 薄膜作为硬掩模, 实现了高深宽比的光栅结构。此外, 针对电感耦合等离子体刻蚀过程中光栅结构出现长草的现象, 通过增强电感耦合等离子体的物理刻蚀机制, 有效消除了结构底部的草状结构。扫描电镜测试结果显示: 将 100 nm 厚 SiO₂ 作为硬掩模, 可以实现周期为 1.00 μm、占空比为 0.45、刻蚀深度为 1.02 μm 的光栅结构, 该光栅结构具有陡直的侧壁形貌以及良好的周期性和均匀性。在该工艺条件下, 电感耦合等离子体刻蚀工艺对 SiO₂ 掩模的刻蚀选择比可达 26.9:1。最后, 将该结构应用于分布式布拉格反射锥形半导体激光器中, 获得了线宽为 40 pm 的激光输出。这表明, 采用电子束光刻技术制备的光栅结构对半导体激光器具有很好的选模特性。

关键词 光栅; 电子束光刻; 邻近效应; 干法刻蚀; 长草现象

中图分类号 TN305.7 文献标志码 A

doi: 10.3788/CJL202249.0313002

1 引言

光栅因能够灵活地实现相位波长变换、相位匹配、耦合等功能, 已被广泛应用于光谱分析^[1]、半导体激光^[2-3]及激光通信^[4]、光电探测^[5]、集成电路^[6]等领域。在传统的法布里-珀罗半导体激光器中加入光栅结构, 可以有效改善半导体激光器的光谱特性, 获得具有波长稳定、窄线宽、单纵模等特性的激光器件。目前, 周期低于 1 μm 的光栅结构被广泛应用于分布式布拉格反射(DBR)半导体激光器^[7]、分布式反馈(DFB)^[8]半导体激光器以及面发射分布式反馈(SE-DFB)^[9]半导体激光器中, 这对其制备工艺提出了严苛要求。光栅的制备方法主要有全息光刻技术^[10]和电子束光刻技术^[11]。相较于全息光刻技术, 电子束光刻技术可以实现亚微米甚至纳米级光刻, 已成为新一代微纳结构加工技术。近年来, 国内外研究机构多采用电子束光刻技术在硅基衬底上制备光栅结构, 例如: 上海交通大学的研究人员^[12]利用电子束光刻技术制备了直径约为 150 nm 的可控硅纳米管, 其直径误差在 3.3% 以内。

电子束光刻技术的分辨率虽然不受衍射效应的限制, 但由于电子在抗蚀剂、衬底中的散射作用, 电子的运动方向被改变, 从而引起另一个影响分辨率的效应——邻近效应^[13]。邻近效应与抗蚀剂、入射条件、衬底条件等有关。在相同的入射条件下, 抗蚀剂越厚、衬底的原子序数越大, 邻近效应就越严重。减小邻近效应常用的方法有几何图形修正技术^[14]、剂量调制方法^[15]及全场邻近效应填平补偿法^[16]。目前, 以上减小邻近效应的方法多被用于硅基衬底的研究上, 较少应用于原子序数更大的 GaAs 基衬底上的研究上。因此, 相比硅基光栅, 采用电子束光刻技术在原子序数更大的 GaAs 衬底上制备微纳光栅更容易受电子束邻近效应的影响, 特别是深刻蚀光栅时需要较厚的抗蚀剂进行掩模, 进一步增大了电子束的邻近效应, 从而导致光栅图形形变、失真。

本课题组基于多层抗蚀剂采用电子束光刻技术和电感耦合等离子体(ICP)刻蚀技术相结合的方法制备深刻蚀的 GaAs 基微纳光栅。较薄的 PMMA A4 抗蚀剂和 SiO₂ 薄膜共同构成电子束光刻的多层抗蚀剂。其中, 较薄的 PMMA A4 抗蚀剂可以有效

收稿日期: 2021-04-27; 修回日期: 2021-05-22; 录用日期: 2021-06-15

基金项目: 吉林省科技发展计划项目(20190302052GX)

通信作者: *fanjie@cust.edu.cn; **mxh@cust.edu.cn

减小光刻中电子束的前向散射, SiO_2 薄膜在减小光刻过程中电子束后向散射的同时,也提升了多层抗蚀剂的抗刻蚀能力。本文还针对 GaAs 基深刻蚀光栅结构长草的现象,分析了草状结构形成的原因以及 ICP 刻蚀工艺参数对光栅形貌的影响,并在优化的 ICP 刻蚀条件下有效消除了草状结构,获得了周期为 $1.00\ \mu\text{m}$ 、占空比为 0.45、刻蚀深度为 $1.02\ \mu\text{m}$ 的光栅结构。

2 实验

采用电子束光刻和 ICP 干法刻蚀技术制备微纳光栅,光刻图形区域尺寸为 $1.0\ \text{mm} \times 0.1\ \text{mm}$,光栅周期为 $1\ \mu\text{m}$,占空比为 0.45,光栅线条长度为 1 mm。本课题组采用 PMMA A4 抗蚀剂和 SiO_2 薄膜共同构成多层抗蚀剂,结合电子束光刻技术、反应离子刻蚀(RIE 刻蚀)技术和 ICP 刻蚀技术,获得了形貌良好的光栅结构,具体工艺流程如图 1 所示。以 GaAs 基外延片为实验基片,将其清洗干净后采用等离子体增强化学气相沉积(PECVD)法蒸镀

$100\ \text{nm}$ 厚 SiO_2 薄膜;之后,将 PMMA A4 抗蚀剂均匀地旋涂在样片表面,在 $4000\ \text{r}/\text{s}$ 的转速下旋涂 $30\ \text{s}$,旋涂后的 PMMA A4 抗蚀剂厚度约为 $400\ \text{nm}$;然后用热板在 $180\ ^\circ\text{C}$ 下前烘 $90\ \text{s}$,以去除其中的有机溶剂,此时 PMMA A4 抗蚀剂和 SiO_2 薄膜共同组成电子束光刻的多层抗蚀剂;接着使用 e-Line 高精度电子束曝光系统进行曝光处理,曝光后用显影液处理 $100\ \text{s}$ (将四甲基二戊酮与异丙醇按 3:1 的体积比配制显影液),显影后用异丙醇定影 $30\ \text{s}$;然后在 $100\ ^\circ\text{C}$ 的热板上坚膜 $60\ \text{s}$,接着以 PMMA A4 抗蚀剂为掩模,采用 Oxford 80+ RIE 设备刻蚀 SiO_2 材料,刻蚀时间 $180\ \text{s}$,将掩模层图形转移到 SiO_2 薄膜上(优化的工艺参数如表 1 所示);最后以样品表面的 SiO_2 作为光栅刻蚀的掩模层,采用 Oxford ICP-180 电感耦合等离子增强反应刻蚀机对样品进行 ICP 干法刻蚀,获得形貌良好的光栅结构。ICP 刻蚀是物理溅射刻蚀和化学刻蚀相结合的工艺,实验中采用 $\text{Cl}_2/\text{BCl}_3/\text{Ar}/\text{N}_2$ 气体^[17] 对 GaAs 基材料光栅进行刻蚀,优化的刻蚀工艺参数如表 2 所示。

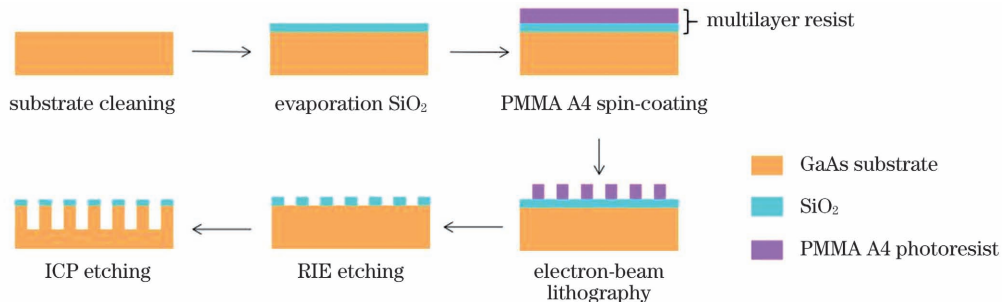


图 1 基于多层抗蚀剂的电子束光刻 GaAs 基微纳光栅的工艺流程图

Fig. 1 Process flow of electron beam lithography GaAs-based micro-nano grating based on multilayer resist

表 1 干法刻蚀 SiO_2 硬掩模的工艺参数

Table 1 Process parameters of dry etching for SiO_2 hard mask

Parameter	Value
Pressure /Pa	2.7
Ratio frequency (RF) power /W	100
CHF_3 flux /($\text{mL}\cdot\text{min}^{-1}$)	72
SF_6 flux /($\text{mL}\cdot\text{min}^{-1}$)	12
Ar flux /($\text{mL}\cdot\text{min}^{-1}$)	5

表 2 ICP 干法刻蚀 GaAs 光栅的工艺参数

Table 2 Process parameters of ICP dry etching for GaAs grating

Parameter	Value
Pressure /Pa	2.0
ICP power /W	500
RF power /W	40–70
Cl_2 flux /($\text{mL}\cdot\text{min}^{-1}$)	10
BCl_3 flux /($\text{mL}\cdot\text{min}^{-1}$)	5
Ar flux /($\text{mL}\cdot\text{min}^{-1}$)	10
N_2 flux /($\text{mL}\cdot\text{min}^{-1}$)	4
Temperature / $^\circ\text{C}$	20

3 分析与讨论

在电子束曝光过程中,因电子束能量很高,粒子性很强,当电子在抗蚀剂中传输和穿透抗蚀剂接触基底表面时,电子束一般会发生两种散射:前向散射和后向散射^[18],如图 2 所示。前向散射一般指电子与抗蚀剂或者基底原子核外层的电子发生的小角度非弹性碰撞,该散射电子的扩展程度主要与抗蚀剂的厚度有关。后向散射是指电子与衬底材料的原子核发生弹性碰撞,这种碰撞会大幅改变电子的运动轨迹。两种散射都会导致曝光图形展宽,特别是对于大面积密集曝光图形来说,大量散射电子会扩展到邻近区域,导致原图形轮廓变形和图形间粘连。

将覆有约 $800\ \text{nm}$ 厚 PMMA A8 抗蚀剂的 GaAs 基外延片表面进行电子束曝光,制备深刻蚀

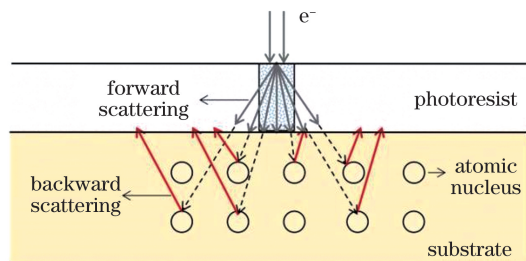


图2 电子束光刻过程中的电子散射示意图

Fig. 2 Schematic of electron scattering in electron beam lithography

的微纳光栅结构。在优化条件下得到的光栅的电镜(SEM)图像如图3(a)所示。可以看出,电子束曝光后的图形不仅存在光栅条粘连现象,部分区域还出现了过曝光现象,整个光栅图形呈现出明显的不均匀性,表现出严重的邻近效应。这主要是因为较厚的PMMA A8抗蚀剂加强了电子的前向散射,同时,前向散射电子到达原子序数较大的GaAs基衬底后增大了电子束的后向散射,进而导致相邻图形合并到一起或者部分区域过度曝光。因此,采用电子束光刻技术制备小周期、长线条、深刻蚀的GaAs基光栅结构时会存在很严重的邻近效应,难以获得良好的光栅掩模图形。

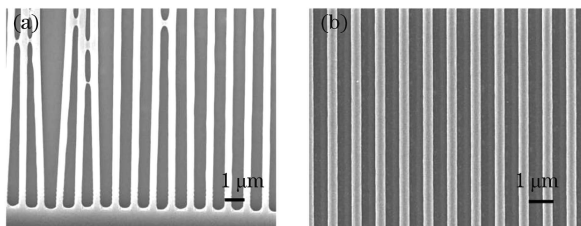


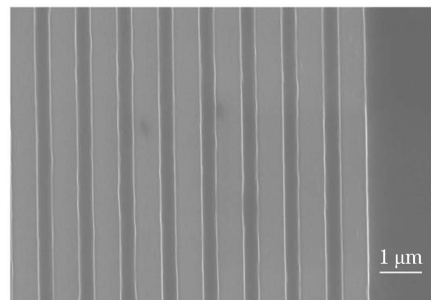
图3 抗蚀剂对光栅光刻胶掩模图形的影响。(a)PMMA A8 抗蚀剂;(b)多层抗蚀剂

Fig. 3 Influences of resists on pattern of grating photoresist mask. (a) PMMA A8 resists; (b) multilayer resist

针对上述问题,本文采用多层次抗蚀剂工艺来减弱电子束曝光过程中的邻近效应。目前研究的多层次抗蚀剂系统主要由灵敏度不同的两层或多层抗蚀剂组成^[19]。本课题组将较薄的PMMA A4抗蚀剂和对电子不敏感的SiO₂薄膜共同构成多层次抗蚀剂,并用其抑制电子束曝光过程中的邻近效应,以获得良好的光栅掩模图形。首先通过控制电子束的曝光剂量使PMMA A4抗蚀剂曝光完全。因抗蚀剂厚度较薄,电子的前向散射范围扩展较小,同时SiO₂薄膜对从衬底后向散射回来的电子具有一定的吸收作用,可减小PMMA A4抗蚀剂中后向散射能量的沉积,从而获得高质量的掩模图形。然后采用图形转

移技术将掩模图形转移到SiO₂薄膜上进行刻蚀。这样既可以减小电子束的邻近效应,又可以实现光栅结构的深刻蚀。图3(b)所示为基于多层次抗蚀剂制备的光栅光刻胶掩模的SEM图像。在优化的曝光剂量($110 \mu\text{C}/\text{cm}^2$)下,结合几何图形修正技术,获得了光栅线宽为435 nm的光栅掩模图形。可以看出,光栅条纹平直清晰,边界对比鲜明,整个光栅图样呈现出良好的均匀性,得到了良好的光栅掩模图形。

以PMMA A4抗蚀剂为掩模,采用RIE刻蚀SiO₂材料。至此,多层次抗蚀剂形成了以SiO₂薄膜为硬掩模的光栅图形。图4为去胶后的SiO₂硬掩模的表面形貌,可以看出制备出的SiO₂光栅掩模边缘齐整、平滑,样品刻蚀区域表面洁净,无残留SiO₂颗粒。

图4 SiO₂ 硬掩模的表面形貌Fig. 4 Surface view of SiO₂ hard mask

以SiO₂为硬掩模,采用ICP刻蚀GaAs基外延片,结果发现光栅槽内存在明显的长草现象。在实际的刻蚀工艺中,造成长草现象的因素有很多,常见的原因包括:掩模的刻蚀残留,刻蚀过程中产生的聚合物过多,来自外界的污染等。上述SiO₂掩模的完好性说明该草状结构是ICP刻蚀过程中掩模被刻蚀产生的颗粒,或者刻蚀过程中产生的不易挥发物等重新沉积在样片表面(形成“微掩模效应”),被等离子体轰击后产生的。因此,需要对ICP刻蚀工艺进行优化,以避免长草现象。

ICP刻蚀是集物理刻蚀和化学刻蚀于一体的十分复杂的反应过程,刻蚀气体流量、腔压P、ICP功率及射频(RF)偏压功率都会对刻蚀结构的形貌造成很大影响。本次实验主要以Cl₂和BCl₃作为刻蚀气体。在高能磁场作用下,气体分子分解成Cl⁺、Cl⁻、Cl、BCl₂、BCl、B⁺等活性粒子和基团参与化学反应,如图5(a)所示。活性中性粒子吸附到材料表面,与表面的GaAs/AlGaAs发生反应Ga+Cl \rightarrow Ga+GaCl_x+GaCl_x⁺(x=0,1,2,3)和As+Cl \rightarrow AsCl_y+AsCl_y⁺+As_z(y=0,1,2,3,4,5;z=0,1,

2,3,4),生成 GaCl_x 、 As_z 等产物^[20-21];此外,ICP刻蚀过程中少量的氧与腔室中的Al元素反应生成的不易挥发的 Al_2O_3 等以及微量 SiO_2 硬掩模颗粒会逐渐沉积在样品表面,如图5(a)~(c)所示。与此同时,等离子体会对样品表面进行轰击,若等离

子体对表面的轰击力度不够,即物理刻蚀机制较弱时,无法有效带走这些沉积物,从而形成了微掩模。在后续ICP刻蚀过程中,这些微掩模会阻挡样品的进一步刻蚀,进而出现长草现象,如图5(d)所示。

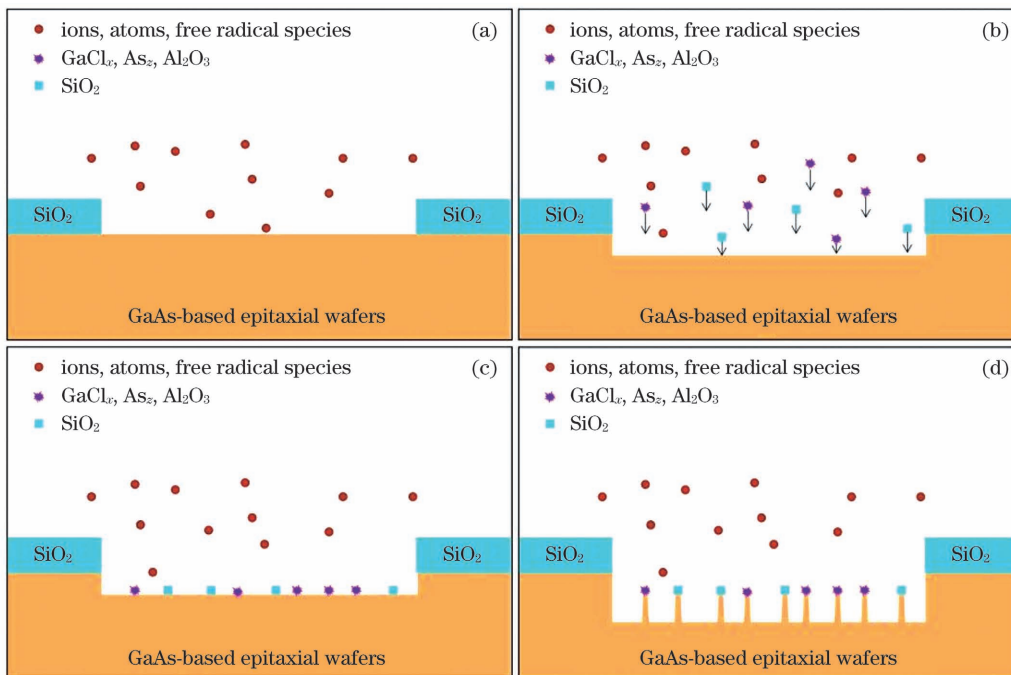


图5 长草现象的生成机制。(a)气体电离;(b)微掩模生成;(c)微掩模沉积;(d)刻蚀

Fig. 5 Generation mechanism of grass phenomenon. (a) Gas ionization; (b) micro-mask generation; (c) micro-mask deposition; (d) etching

在优化的气体配比条件下,通过提高RF偏压功率,增强ICP的物理刻蚀机制^[20],可以在保证光栅侧壁形貌良好的同时,有效改善光栅结构底部的长草现象。图6所示为不同RF偏压功率下刻蚀70 s的光栅SEM图。从图中可以看出,随着ICP刻蚀工艺中RF偏压功率的增大,光栅槽内的草状

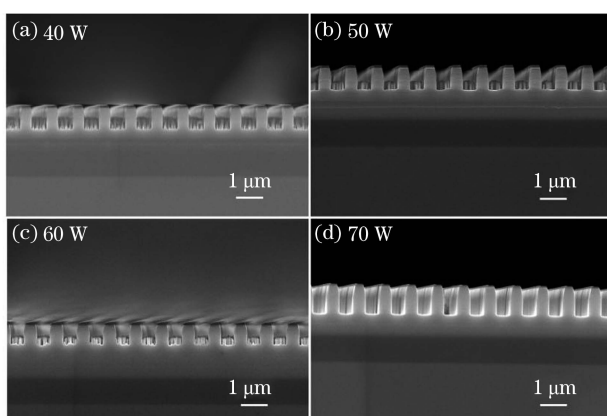


图6 不同RF偏压功率下的光栅截面图

Fig. 6 Cross-sectional views of grating with different RF powers

结构逐渐减少,在RF偏压功率为70 W时完全消失。这主要是因为随着RF偏压功率的增加,等离子体能量增加,物理轰击样品表面的作用加强,吸附在样品表面阻挡刻蚀的生成物被等离子体从基片表面轰击脱落的概率增大,进而减弱了长草效应。但是,RF偏压功率的增大也加大了对 SiO_2 硬掩模的刻蚀力度,导致掩模梯形化,进而使得光栅结构顶端逐渐钝角化。在优化的ICP工艺条件下获得了周期为 $1.00 \mu\text{m}$ 、占空比为0.45、深度为 $1.02 \mu\text{m}$ 的光栅图形,光栅侧壁陡直、缺陷少,而且占空比的一致性好,将其应用于半导体激光器可以有效提升器件的成品率。

进一步分析RF偏压功率对光栅、草状结构以及 SiO_2 硬掩模的影响,结果如图7所示。从图7(a)中可以看出:随着RF偏压功率增大,草状结构与光栅的深度比逐渐减小,而光栅的刻蚀深度则先缓慢增大后急剧增大;在RF功率为70 W时,草状结构消失,光栅的刻蚀深度(去除 SiO_2 掩模后)达到了 $1.02 \mu\text{m}$ 。这主要是因为RF偏压功率较低

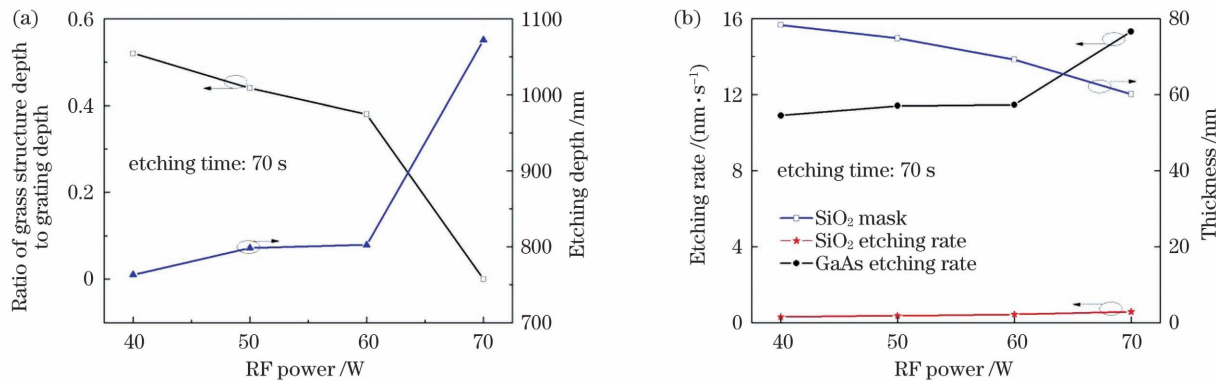


图 7 RF 偏压功率对光栅、草状结构、 SiO_2 硬掩模的影响。(a) 对光栅刻蚀深度以及草状结构深度与光栅深度之比的影响;(b) 对 GaAs 和 SiO_2 掩模刻蚀速率及 SiO_2 掩模厚度的影响

Fig. 7 Effects of RF power on grating, grass structure, and SiO_2 hard mask. (a) Effects on grating etching depth and the ratio of grass structure depth to grating depth; (b) effects on GaAs and SiO_2 mask etching rate and SiO_2 mask thickness

时,等离子体中离子的能量不足以移除样品表面的微掩模,残余的微掩模使得反应气体无法充分地与样品材料接触发生化学刻蚀,从而阻碍了 GaAs 的进一步刻蚀。当 ICP 刻蚀的 RF 偏压功率足够大时,物理刻蚀机制增强,不仅可以移除样品表面的微掩模,还会使刻蚀气体与被刻蚀材料充分接触并打断被刻蚀材料的化学键,增强材料的化学刻蚀,因此 GaAs 的刻蚀深度急剧增大。图 7(b)所示为 RF 偏压功率对 GaAs 和 SiO_2 掩模刻蚀速率及 SiO_2 掩模剩余厚度的影响,其中刻蚀速率是通过 SEM 测试的刻蚀深度与刻蚀时间的比值计算得到的。从图中可以看出:当 RF 偏压功率小于 70 W 时,由于微掩模的存在,GaAs 的刻蚀速率缓慢增大,在 RF 偏压功率为 70 W 时,微掩模的消失导致 GaAs 的刻蚀速率急剧增大,达到 15.31 nm/s。此外,随着 RF 功率增大, SiO_2 刻蚀速率也是缓慢增大的,当 RF 功率为 70 W 时, SiO_2 掩模的剩余厚度仍有 60 nm。此时,ICP 刻蚀工艺对 SiO_2 掩模的选择比达到了 26.9:1,可以获得高深宽比的光栅结构。

将上述制备的微纳光栅结构作为 DBR 光栅应用于锥形半导体激光器中。该半导体激光器中 DBR 光栅和脊型波导的长度均为 1 mm,锥形放大区的长度为 1.5 mm,如图 8 内插图所示。DBR 光栅的周期为 1.00 μm ,占空比为 0.45,深度为 1.02 μm ,脊型波导宽度为 5 μm ,锥形放大区锥角为 5°。器件制备完成后,在前腔面和后腔面分别蒸镀反射率为 2% 和 96% 的腔面膜,然后 P 面向上封装在 CuW 热沉上,进行光谱测试。光谱测试用设备为 YOKOGAWA AQ6370D 光谱仪,其分辨率可达到 20 pm。在脊型波导电流为 400 mA、锥形区电

流为 900 mA、温度为 20 °C 时测得的器件的发射光谱如图 8 所示。可以看出,激光器的输出波长为 1057.69 nm,其边模抑制比可达 36 dB,3 dB 线宽仅为 40 pm。这表明将所制备的微纳光栅结构应用于半导体激光器中可以实现窄线宽、高边模抑制比的激光输出。

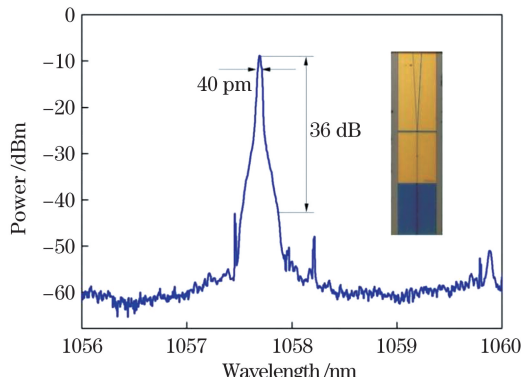


图 8 激光器的光谱图

Fig. 8 Spectrum of laser

4 结 论

本课题组采用电子束光刻技术和 ICP 刻蚀技术相结合的方法制备深刻蚀的 GaAs 基微纳光栅结构。针对制备小周期、长线条、深刻蚀 GaAs 基光栅过程中,电子束曝光产生严重的邻近效应进而导致光栅掩模图形出现形变、失真的问题,本课题组将较薄的 PMMA A4 抗蚀剂和 SiO_2 薄膜作为多层抗蚀剂来有效降低电子散射的扩展范围,减小电子束的邻近效应。实验结果显示,该方案获得了良好光刻胶掩模图形,同时,将 SiO_2 薄膜作为硬掩模实现了光栅结构的深刻蚀。

通过优化 ICP 的 RF 功率来调节 ICP 的物理刻蚀机制,消除了 ICP 刻蚀过程中出现的长草现象。在优化的工艺条件下,获得了周期为 $1.00\text{ }\mu\text{m}$ 、占空比为 0.45、刻蚀深度为 $1.02\text{ }\mu\text{m}$ 的光栅结构。在此刻蚀深度下,光栅的侧壁陡直,且具有良好的周期性和均匀性。同时,ICP 刻蚀工艺对 SiO_2 掩模的选择比可达到 26.9:1,可实现高深宽比的 GaAs 基微纳光栅结构。该工艺为使用电子束光刻技术制备深刻蚀、高深宽比的 GaAs 基微纳结构提供了参考。将该微纳光栅结构应用 DBR 锥形半导体激光器中,获得了波长为 1057.69 nm、3 dB 线宽为 40 pm、边模抑制比为 36 dB 的激光输出。

参 考 文 献

- [1] Diba A S, Xie F, Gross B, et al. Application of a broadly tunable SG-DBR QCL for multi-species trace gas spectroscopy[J]. Optics Express, 2015, 23(21): 27123-27133.
- [2] Li L Y, Shi Y C, Zhao Y, et al. Transverse modal control of wide-stripe high power semiconductor lasers using sampled grating [J]. Optics Express, 2018, 26(9): 11171-11180.
- [3] Müller A, Fricke J, Bugge F, et al. DBR tapered diode laser with 12.7 W output power and nearly diffraction-limited, narrowband emission at 1030 nm [J]. Applied Physics B, 2016, 122(4): 1-6.
- [4] Lu D, Yang Q L, Wang H, et al. Review of semiconductor distributed feedback lasers in the optical communication band [J]. Chinese Journal of Lasers, 2020, 47(7): 0701001.
陆丹, 杨秋露, 王皓, 等. 通信波段半导体分布反馈激光器[J]. 中国激光, 2020, 47(7): 0701001.
- [5] Zhang R, Fu Z L, Gu L L, et al. Terahertz quantum well photodetectors with reflection-grating couplers [J]. Applied Physics Letters, 2014, 105(23): 231123.
- [6] Bickford J R, Cho P S, Farrell M E, et al. The investigation of subwavelength grating waveguides for photonic integrated circuit based sensor applications [J]. IEEE Journal of Selected Topics in Quantum Electronics, 2019, 25(3): 1-10.
- [7] Spießberger S, Schiemangk M, Wicht A, et al. DBR laser diodes emitting near 1064 nm with a narrow intrinsic linewidth of 2 kHz [J]. Applied Physics B, 2011, 104(4): 813-818.
- [8] Gao F, Qin L, Chen Y Y, et al. Study of gain-coupled distributed feedback laser based on high order surface gain-coupled gratings [J]. Optics Communications, 2018, 410: 936-940.
- [9] Jin Y, Gao L, Chen J, et al. High power surface emitting terahertz laser with hybrid second-and fourth-order Bragg gratings [J]. Nature Communications, 2018, 9(1): 1407.
- [10] Gong C Y, Fan J, Zou Y G, et al. Fabrication of holographic lithography micro-nano gratings using metal mask [J]. Chinese Journal of Lasers, 2019, 46(12): 1203001.
龚春阳, 范杰, 邹永刚, 等. 基于金属掩模的全息光刻微纳光栅制备工艺[J]. 中国激光, 2019, 46(12): 1203001.
- [11] Okazaki S. High resolution optical lithography or high throughput electron beam lithography: the technical struggle from the micro to the nano-fabrication evolution [J]. Microelectronic Engineering, 2015, 133: 23-35.
- [12] Wang X D, Xu J, Quan X L, et al. Fast fabrication of silicon nanopillar array using electron beam lithography with two-layer exposure method [J]. Microelectronic Engineering, 2020, 227: 111311.
- [13] Chang T H P. Proximity effect in electron-beam lithography [J]. Journal of Vacuum Science and Technology, 1975, 12(6): 1271-1275.
- [14] Klimpel T, Schulz M, Zimmermann R, et al. Model based hybrid proximity effect correction scheme combining dose modulation and shape adjustments [J]. Journal of Vacuum Science & Technology B, 2011, 29(6): 06F315.
- [15] Yang-Keathley Y, Maloney S A, Hastings J T. Real-time dose control for electron-beam lithography [J]. Nanotechnology, 2021, 32(9): 095302.
- [16] Mack C A. Electron-beam lithography simulation for mask making: VI. Comparison of 10- and 50-kV GHOST proximity effect correction [J]. Proceedings of SPIE, 2001, 4409: 194-203.
- [17] Vigneron P B, Joint F, Isac N, et al. Advanced and reliable GaAs/AlGaAs ICP-DRIE etching for optoelectronic, microelectronic and microsystem applications [J]. Microelectronic Engineering, 2018, 202: 42-50.
- [18] Manfrinato V R, Zhang L H, Su D, et al. Resolution limits of electron-beam lithography toward the atomic scale [J]. Nano Letters, 2013, 13(4): 1555-1558.
- [19] Sarkar M, Mohapatra Y N. Self-aligned electron beam lithography of metallic layer sandwiched in a polymer multilayer: facilitation of vertical organic transistor fabrication [J]. Microelectronic Engineering, 2014, 115: 16-20.
- [20] Wang Y, Zhou Y P, Li M L, et al. ICP etching process of GaAs/AlGaAs for vertical-cavity surface-emitting lasers [J]. Chinese Journal of Lasers, 2020, 47(4): 0401005.

- 王宇, 周燕萍, 李茂林, 等. 用于垂直腔面发射激光器的 GaAs/AlGaAs 的 ICP 刻蚀工艺研究 [J]. 中国激光, 2020, 47(4): 0401005.
- [21] Kao C C, Huang H W, Tsai J Y, et al. Study of dry etching for GaN and InGaN-based laser structure using inductively coupled plasma reactive ion etching [J]. Materials Science and Engineering B, 2004, 107 (3): 283-288.

Deep Etching Process of GaAs-Based Micro-Nano Grating Based on Multilayer Resist

Yang Jingjing^{*}, Fan Jie^{**}, Ma Xiaohui^{**}, Zou Yonggang, Wang Qiqi

State Key Laboratory of High Power Semiconductor Laser, Changchun University of Science and Technology, Changchun, Jilin 130022, China

Abstract

Objective Due to its high-resolution and precision pattern generation technology, electron-beam lithography has become a new generation of micro-nano structure processing technology; however, the proximity effect will cause deformation and distortion of the mask pattern. The common methods to solve the proximity effect include shape correction, dose modulation, and global horizontal sounding technique. Now, the above methods for solving the proximity effect are mostly used in studies on silicon substrates; however, relatively few studies on GaAs substrates with high atomic numbers have been published. Compared with silicon-based gratings, the use of electron-beam lithography to fabricate micro-nano gratings on GaAs substrates with larger atomic numbers is more susceptible to proximity effects. Deep etching of the grating, in particular, necessarily involves a thicker masking resist, which increases the proximity effect of the electron beam and makes good mask patterns difficult to obtain.

Methods The electron-beam lithography technology was used to prepare deeply etched GaAs-based micro-nano gratings based on a multilayer resist process in this paper. Plasma enhanced chemical vapor deposition was used to construct a 100 nm thick SiO₂ layer on the surface of the epitaxial wafer, and then a 400 nm thick PMMA A4 resist layer was spin-coated on top of the SiO₂. Then, PMMA A4 resist and SiO₂ film formed a multilayer resist for electron-beam lithography. After that, a grating structure was obtained by combining electron-beam lithography, reactive ion etching (RIE) etching, and inductively coupled plasma (ICP) etching. Then, the morphology of the surface and cross section of the grating structure was analyzed using a scanning electron microscope. The reasons for the formation of grass in the grating groove during the ICP etching process were investigated to understand the grass phenomenon. The effect of ratio frequency (RF) bias power on grass, grating, and SiO₂ film was investigated further. In addition, the grating structure was used as a distributed Bragg reflection (DBR) grating in the tapered diode laser, and the spectral characteristics of the device were tested to characterize the properties of the grating structure.

Results and Discussions The grating structure with a period of 1.00 μm, a duty cycle of 0.45, and a depth of 1.02 μm is successfully fabricated using a multilayer resist process. In electron-beam lithography, the thin PMMA A4 resist effectively reduces forward scattering, whereas the SiO₂ film effectively reduces backward scattering, resulting in high-quality mask patterns [Fig. 3(b)]. Then, the mask pattern is transferred to the SiO₂ film by RIE etching technology (Fig. 4), which provides an effective barrier for the deep etching of the grating structure. The grass phenomenon is discovered at the bottom of the grating structure during the ICP etching process. The presence of micro-masks is thought to cause the grass phenomenon based on the analysis of reasons for the occurrence of grass phenomenon (Fig. 5). In the case of optimized gas ratio, the physical etching mechanism of ICP enhances by increasing the RF bias power, and effectively eliminates the grass (Fig. 6). This study demonstrates that when the RF bias power is low, the physical etching mechanism is weak, and the presence of a micro-mask prevents further etching of GaAs [Fig. 7(a)]. When the RF bias power is increased to 70 W, the micro-mask disappears and the etching rate of GaAs increases dramatically, and the selection ratio of the ICP etching process to the SiO₂ mask reaches 26.9:1 [Fig. 7(b)]. Finally, the micro-nano grating structure is applied to the DBR tapered diode laser, and the laser output with a wavelength of 1057.69 nm, a side mode suppression ratio of 36 dB, and a linewidth of

40 pm was obtained (Fig. 8).

Conclusions In this paper, deep etched GaAs-based micro-nano grating structures are prepared using a combination of electron-beam lithography and ICP etching technology. Electron-beam exposure deforms and distorts the mask pattern for GaAs-based gratings with small periods, long lines, and deep etching depth due to the severe proximity effect. Using thin PMMA A4 resist and SiO₂ film as multilayer resist, the spread range of electron scattering is effectively decreased and the proximity effect of an electron beam is reduced. A good photoresist mask pattern is obtained in this scheme, and the SiO₂ film is used as a hard mask to achieve deep grating etching. Furthermore, the grass phenomenon during the ICP etching process is eliminated by optimizing the RF power and adjusting the physical etching mechanism. Under optimized process conditions, the grating structure with a period of 1.00 μm, a duty cycle of 0.45, and an etching depth of 1.02 μm is obtained, and the sidewall of the grating is steep and has good periodicity and uniformity. Simultaneously, the ICP etching process's selection ratio to the SiO₂ mask can reach 26.9:1, allowing for the realization of a GaAs-based micro-nano grating structure with a high aspect ratio. This process provides a reference for the use of electron-beam lithography to prepare deeply etched, high-aspect-ratio GaAs-based micro-nano structures. Finally, the structure is applied to a DBR tapered semiconductor laser, and a laser output with a line width of 40 pm was obtained, indicating that the grating structure created by this process has good model selection performance for the semiconductor laser.

Key words gratings; electron-beam lithography; proximity effect; dry etching; grass phenomenon